Article

Effect of the Field-Stress State on the Subgrade Resilient Modulus for Pavement Rutting and IRI

Kazi Moinul Islam * and Sarah L. Gassman

Civil and Environmental Engineering, University of South Carolina, Columbia, SC 29208, USA;
gassman@cec.sc.edu
* Correspondence: kislam@email.sc.edu; Tel.: +1-803-360-3836

Abstract: The new Mechanistic-Empirical Pavement Design Guide (MEPDG) uses the subgrade resilient modulus (M_R) as the key input parameter to represent the subgrade soil behavior for pavement design. The resilient modulus increases with an increase in confining pressure, whereas, for an increase in deviatoric stress, it increases for granular soils and decreases for fine-grained soils. The value of M_R is highly stress dependent, with the stress state (i.e., bulk stress) a function of the position of the materials in the pavement structure and applied traffic loading. Applying excessive vertical stress at the top of the subgrade without knowing the appropriate stress state can result in permanent deformation. In situ stress must be calculated so the correct resilient modulus can be determined. To facilitate the implementation of MEPDG, this study develops a methodology to select the appropriate subgrade resilient modulus for predicting rutting and IRI. A comprehensive research methodology was undertaken to study the effect of in situ or undisturbed subgrade M_R on pavement performance using the MEPDG. Results show that M_R obtained from in situ stress is approximately 1.4 times higher than the M_R estimate from NCHRP-285. Thus, the in situ stress significantly affects the calculation of subgrade M_R and, subsequently, the use of M_R in the predicted rutting, with IRI using the AASHTOWare pavement mechanistic-empirical design. Results also show that the pavement sections were classified as in "Good" and "Fair" conditions for rutting and IRI, respectively, considering in situ M_R.

Keywords: MEPDG; resilient modulus; rutting; IRI; in situ stress

1. Introduction

The new guide for the mechanistic-empirical design of new and rehabilitated pavement structures (M-E Design Guide) and the 1993 guide for the design of pavement structures of the American Association of State Highway and Transportation Officials (AASHTO) recommend the use of resilient modulus (M_R) of base and subgrade materials for pavement design and analysis [1–3]. M_R is the ratio of the applied deviator stress (σ_d) to the resilient strain (ε_r) [4]. It represents the stiffness of the pavement unbound layer configuration subjected to repeated traffic loading. It is the primary input for the subgrade soil in MEPDG and is essential for computing stresses, strains, and deformations in pavement structures induced by applied traffic loads [5–10]. Laboratory test methods include the repeated load triaxial test (RLTT) (AASHTO-T307-99 2017) [11], the most commonly used method for determining the resilient modulus of subgrade soils.

The RLTT test is commonly used to measure the resilient modulus of subgrade soils in the laboratory [12–18]. This test is designed to simulate the stress induced by traffic loading through a series of cyclic deviator stresses applied to the specimen at different confining pressures [13]. Seed, Mitry, Monismith, and Chan [19] found that the stress variables (e.g., bulk stress, deviator stress, and octahedral stress) significantly affect the resilient modulus. Several models have been built to predict the resilient modulus of subgrade soils using bulk stress, deviatoric stress, or a combination [20–25]. The bulk stress, which includes

the confining pressure and deviator stress, is used by most resilient-modulus prediction models. For example, when the bulk stress is 70 kPa, the deviator stress and confining pressure can be 40 kPa and 10 kPa, respectively, and the deviator stress and confining pressure can be 10 kPa and 20 kPa, respectively. The value of the bulk stress is the same, but the stress state is different. The models need to better reflect the effect on the bulk stress under various combinations of the confining pressure and deviator stress. The deviator and bulk-stress models are classified as the two-parameter models and are generally used for cohesive and granular soils, respectively. The three-parameter models, such as octahedral stress and the universal model, are used for cohesive and granular soils [26,27].

Predicting flexible pavement performance is highly dependent on the accuracy of the M_R value. Islam and Gassman (2023) [28] found that the laboratory-measured M_R obtained using the stress state in NCHRP-285 predicted higher rutting than the M_R back calculated from FWD testing and PMED v2.6.2.2 default values. The rutting predicted from the laboratory-measured M_R exceeded the field-measured distress but was below the design threshold. Furthermore, the least amount of AC top-down cracking was predicted for pavements with fine-grained subgrade soils when using the laboratory-measured M_R. Rada and Witczak (1981) [29] suggested that the applied stress level influenced the M_R. It is important to note that the resilient modulus for subgrade soils is highly stress dependent, with the stress state being a function of the position of the material in the pavement structure and applied traffic loading [30]. The M_R of fine-grained soil generally decreases with increasing deviatoric stress (this is referred to as 'stress-softening' behavior; with increased stress, deformation increases and modulus decreases), whereas the M_R of coarse-grained soils generally increases with increasing deviatoric stress (this is referred to as the 'strain-hardening' effect due to the reorientation of the grains into the denser state) [30–34]. Model forms characterizing the relationship between M_R and deviatoric stress are bi-linear, hyperbolic, semi-log, and log-log [35–37]. To properly investigate the "strain-hardening" and "stress-softening" effect of coarse-grained and fine-grained soils, a field-stress state should be considered for determining M_R for a typical pavement structure and traffic loading.

To date, limited research has been conducted to evaluate the influence of the methodology used to estimate in situ M_R for subgrade soils. Thus, this study calculated an in situ stress state from the existing pavement conditions to overcome the issue. Eleven Asphalt Concrete (AC) pavement sections were available for this study, and 73 boreholes were used to characterize the subgrade soils and develop a correlation between laboratory-measured M_R per NCHRP-285 [38] "$M_{R(285)}$" and in situ subgrade M_R from the field- stress state "$M_{R(in\ situ)}$". A research study was undertaken to investigate the effect of field stress on subgrade M_R and predict pavement rutting and IRI for flexible pavement. The resilient modulus test results were examined to determine how confining pressure and deviator stress affected the soil's resilient behavior. A summary of the findings is given to understand better the resilient properties of the in situ stress state of subgrade soil.

2. Research Questions and Objectives

Three research questions were addressed to fulfill the overall research objectives of this study.

1. What is the effect of the stress conditions on the calculated M_R for subgrade soil?
2. How does the subgrade M_R affect the predicted rutting and IRI?
3. Is it possible to classify pavement conditions based on predicted and measured pavement performance?

To address these research questions, the following research work was completed:

- Task 1: Conduct Repeated Load Triaxial Test (RLTT) as per AASHTO T307 (AASHTO 2017) for coarse-grained and fine-grained samples.
- Task 2: Obtain laboratory-measured M_R ($M_{R(285)}$) as per NCHRP-285 [38] and in situ M_R ($M_{R(in\ situ)}$) using field-stress conditions. Establish a linear relationship between the

$M_{R(285)}$ and $M_{R(\text{in situ})}$ and estimate the Pearson product-moment correlation coefficient (r). The value of r can range from 0.0, indicating no relationship between the two variables, to positive or negative 1.0, indicating a strong linear relationship between the two variables. Bias and Standard Error of Estimate (SEE) were also calculated.

- Task 3: Predict rutting and IRI using MEPDG and compare them with field-measured values. Classify the pavement conditions as "Good", "Fair", and "Poor" as per FHWA guidelines [39] for rutting and IRI.

3. Research Methodology

The primary variable to be investigated in this study is the subgrade resilient modulus, M_R, that will be used to predict pavement rutting, and IRI, using the AASHTOWare PMED software (v2.6.2.2). Repeated load triaxial tests were performed in the laboratory using AASHTO T307, and the M_R was obtained from two different methods: (1) using the stress conditions per NCHRP-285 ($M_{R(285)}$) and (2) considering the in situ stress ($M_{R(\text{in situ})}$). Data for 11 asphalt concrete (AC) pavement sections in South Carolina were used in this study (see Table 1). Table 1 tabulates the construction finish year, pavement length, and number of Shelby tube samples for each section. A total of 73 samples of subgrade soil were collected for this study. Pavement sections B278 and L72 will be used to illustrate the methodology. B278 has coarse-grained subgrade soil, and L72 has fine-grained subgrade soil.
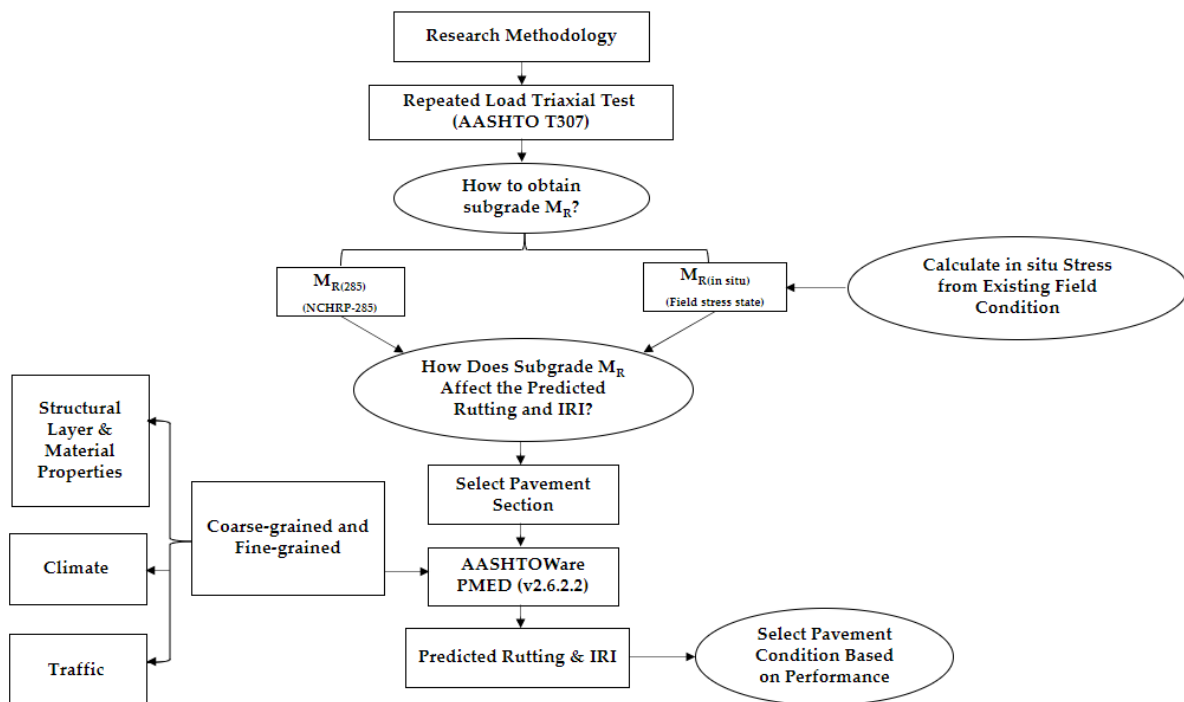
Table 1. Summary of Pavement Sections.

Site ID	Construction Finish Year	Length of Section (km)	Number of Coring Locations with Shelby Tube Samples
B278	1998	2.6	3
C461	1996	4.0	3
C9	1999	3.0	3
C151	1999	8.7	10
F327	1992	7.9	6
G521	2003	4.8	7
H22	2001	1.6	3
H31	2005	6.4	9
O321	2004	9.8	13
L72	2002	9.8	11
P93	2001	1.9	5

Note: B278 = Beaufort/US-278, C461 = Charleston/SC-461, C9 = Chester/SC-9, C151 = Chesterfield/SC-151, F327 = Florence/SC-327, G521 = Georgetown/US-521, H22 = Horry/SC-22, H31 = Horry/SC-31, O321 = Orangeburg/US-321, L72 = Laurens/SC-72, P93 = Pickens/SC-93.

At each pavement site, the pavement was cored, layer thicknesses were measured, and samples of subgrade soil were collected from beneath the pavement. Shelby tube samples were used to determine the resilient modulus per AASHTO T307. A hand auger was used to collect bulk samples from each borehole. Tests performed include Atterberg Limits (ASTM D 4318/AASHTO T 89 and T 90), grain size analysis (ASTM D 421 and D 422/AASHTO T 87 and T 88), soil classification (ASTM D 2487/AASHTO M 145), specific gravity (ASTM D 854/AASHTO T 100), moisture content (ASTM D 2216-90/AASHTO T 265), and standard Proctor compaction (ASTM D 698-78/AASHTO T 99-90).
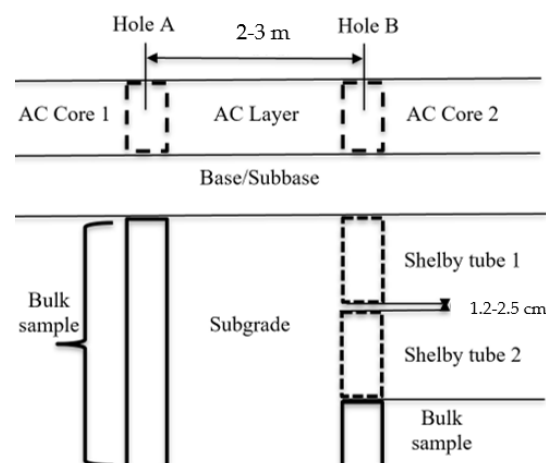
Figure 1 illustrates how subgrade M_R obtained by the two methods was used as input to the AASHTOWare PMED process. Using the PMED software (v2.6.2.2), the rutting and IRI were predicted for each trial pavement section based on subgrade M_R values and compared with the measured field values. Finally, the pavement section condition was classified per FHWA [39].
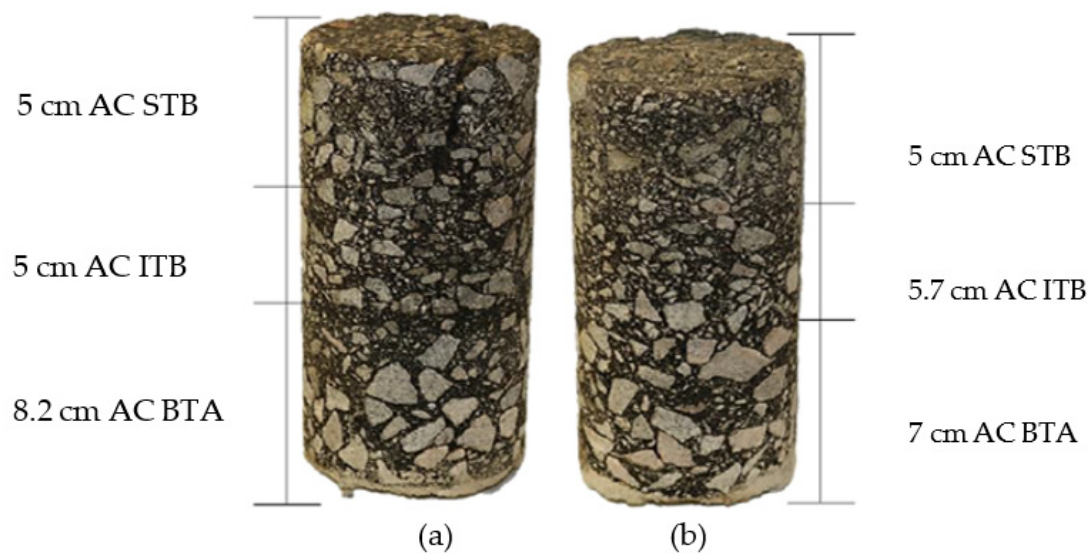
Figure 1. Study Flow Chart.

3.1. Pavement Profile Layer Information

Pavement profiles for eleven sites in South Carolina were obtained from field investigations that included drilling and sampling of the subsurface soils between 2015 and 2021. Two holes were cored for each boring location (see Figure 2). Hole A corresponds to a location on the pavement surface that was free of visible surface distress ("non-distressed"), while Hole B corresponds to a location with surface distress ("distressed"). The core length was measured after extraction, and the number of layers of different asphalt mixture types within the AC layer was identified (see Figure 3). The base/subbase thickness measurements were obtained after extracting the asphalt core. The thickness of each layer and the corresponding unit weight for each borehole along sections B278 and L72 are summarized in Table 2. Each pavement section is divided into segments based on the number of boreholes along each section. For example, B278 has 3 segments, B278–1, B278–2 and B278–3. The detailed procedures used to collect the thin-walled Shelby tube and bulk soil samples are documented in Islam and Gassman (2023) [28]. Note that the AC thickness of Hole A was used to calculate in situ stress.

Figure 2. Schematic Diagram Showing Coring and Sampling Locations with Depth.

Figure 3. Photographs of Asphalt Cores from B278 (BH-1): (**a**) Hole B and (**b**) Hole A [41].

Table 2. Summary of Pavement Profile Information.

Site ID	BH	Asphalt Core		Unit Weight $\gamma 1$ (kN/m³)	Base Layer		Subgrade Layer	
		Thickness (cm)			Thickness (cm)	Unit Weight $\gamma 2$ [a] (kN/m³)	Thickness (cm)	Unit weight $\gamma 3$ [b] (kN/m³)
		Core 1 (Hole A)	Core 2 (Hole B)					
B278	B278-1	17.7	18.2		15.2		15.4	16.8
	B278-2	19.1	19.1		16.5	20.3	16.5	16.9
	B278-3	15.2	15.2		17.8		17.3	17.6
L72	L72-1	16.5	16.5	STB = 22.3 ITB = 22.6 BTA = 22.8	10.2	22.2	16.2	16.9
	L72-2	16.8	16.8		12.7		15.7	16.9
	L72-3	36.8	35.6		No base		16.3	16.9
	L72-4	17.8	17.8		12.7		16.5	16.9
	L72-5	16.5	15.2		11.4		17.0	17.4
	L72-6	17.8	17.8		10.2		16.2	16.9
	L72-7	29.2	25.4		No base		16.2	16.9
	L72-8	25.4	25.4		No base		17.3	18.4
	L72-9	27.3	26.0		No base		17.4	18.4
	L72-10	29.2	25.4		No base		17.3	18.4
	L72-11	29.8	27.9		No base		16.7	17.3

Note: $\gamma 1$ = average of STB, ITB, and BTA, STB = Surface Type B, ITB = Intermediate Type B, BTA = Base Type A (this average value depends on the layer type, and corresponding unit weights were used), [a] Base unit weight obtained from Amirkhanian and Corley [40]. [b] Natural unit weight determined from Shelby tube samples.

3.2. Resilient Modulus Tests

Resilient modulus (M_R) tests were performed on the 76 mm-diameter by 152 mm-long specimens obtained from thin-walled Shelby tubes. A GDS Advanced Dynamic Triaxial Testing System performed the tests per AASHTO T 307.

The subgrade M_R was obtained using the constitutive model in Equation (1) (NCHRP-1-37A, 2004) [42]:

$$M_R = k1 P_a \left(\frac{\theta}{P_a} \right)^{k2} \left(\frac{\tau_{oct}}{P_a} + 1 \right)^{k3} \tag{1}$$

where

P_a = atmospheric pressure (101.1 kPa)
k1, k2, and k3 = model parameters
θ = bulk stress = $(\sigma_1 + \sigma_2 + \sigma_3)$
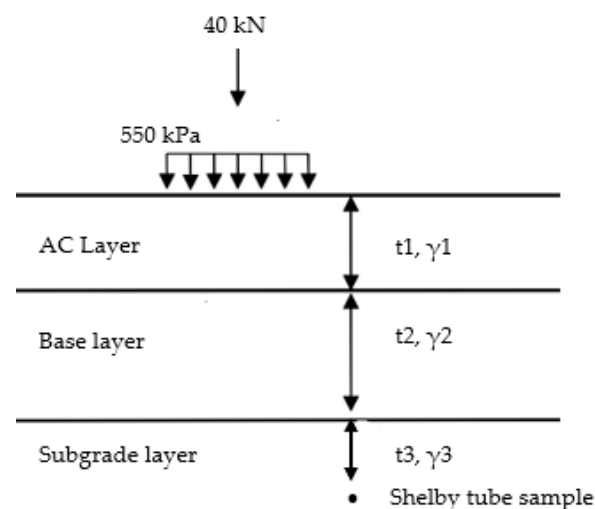σ_1, σ_2, and σ_3 = principal stresses and
τ_{oct} = octahedral shear stress

$$= \sqrt{(\sigma_1 - \sigma_2)^2 + (\sigma_1 - \sigma_3)^2 + (\sigma_2 - \sigma_3)^2}/3$$

After completing the M_R testing procedure (see Islam and Gassman (2023) [28] for details), the M_R was calculated for 15 sequences per AASHTO T307. For determining k1, k2, and k3, Equation (1) was simplified and transferred to the logarithmic function. Two approaches were used to estimate the M_R: (1) using the stress state recommended by NCHRP-285 and (2) using the in situ stress state. First, the laboratory-measured resilient modulus ($M_{R(285)}$) was calculated using Equation (1) with confining stress (σ_3) equal to 14 kPa and cyclic stress (deviator) equal to (σ_d) 41 kPa per NCHRP-285 (2004). Second, the laboratory-measured resilient modulus for the in situ stress state ($M_{R\ (in\ situ)}$) was calculated using Equation (1) with confining stress (σ_3) and cyclic stress/deviator (σ_d) stress calculated from the in situ stress state.

3.3. Calculate In Situ Stress for the Existing Pavement Section

As shown in Figure 4, each pavement section consists of a t1 cm-thick Asphalt Concrete (AC) layer overlying a t2 cm-thick base layer and a t3 cm-thick layer of subgrade soil. The t1 thickness consists of up to 3 layers (STB, ITB, and BTA in Figure 3), and the unit weight of these layers was obtained from laboratory testing (AASHTO T166). The value of the unit weight is 22.3 kN/m^3 for STB, 2.6 kN/m^3 for ITB, and 22.8 kN/m^3 for BTA. An average of these values was used to represent the unit weight of the AC layer. The base unit weight was obtained from Amirkhanian and Corley [40], and the subgrade unit weight was obtained from measurements of the Shelby tube samples. The values are summarized in Table 2.

Figure 4. Schematic Pavement Profile for AC under Wheel Loading.

A 40 kN load was considered to simulate the conditions used in the design process. The 40 kN load level is equivalent to a tire inflation pressure of 520 to 550 kPa (per AASHO 1972) and was used for the analysis.

The total vertical stress acting on the soil sample is the sum of the vertical stresses from the pavement structure (σ_{1pave}) and the applied load (σ_{1load}). Similarly, the total horizontal stress is the sum of the horizontal stresses from the pavement structure (σ_{3pave}) and the applied load (σ_{3load}). The groundwater table was not encountered during sampling, so

total and effective stress are considered equal. Equations (2) and (3) present the calculations for the vertical and horizontal stress from the pavement structure.

$$\sigma_{1pave} = \left(t1 \times \gamma1 + t2 \times \gamma2 + t3 \times \gamma3 \right), \ kN/m^2 \tag{2}$$

where t is the thickness (m), and γ is the unit weight (kN/m^3). These values were obtained through field investigations and are summarized in Table 2.

$$\sigma_{3pave} = k_0 \times \sigma_{1pave}, \ kN/m^2 \tag{3}$$

where $k_0 = 0.5$ [43].

When the load is applied over a single circular loaded area, the most critical stress-strain and deflection occur under the center of the circular area on the axis of symmetry, where $\tau_{rz} = 0$ and $\tau_{rz} = 0$, so $\sigma_r = \sigma_t$ are the principal stresses [43] σ_r and σ_t similar to a flexible plate with a radius α and a uniform pressure q. The stresses beneath the center of the plate can be determined from Equations (4) and (5) [43].

$$\sigma_z = q \left[1 - \frac{z^3}{\left(a^2 + z^2 \right)^{1.5}} \right] \tag{4}$$

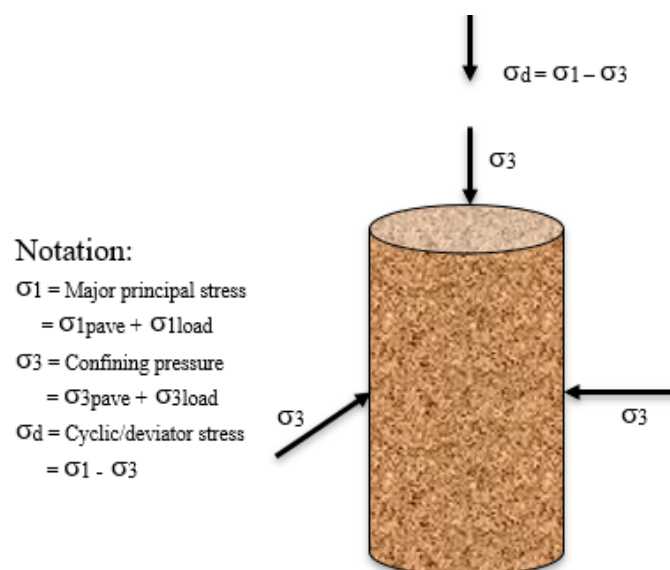$$\sigma_r = q/2 \left[1 + 2\nu - \frac{2(1+\nu)z}{\left(a^2 + z^2 \right)^{0.5}} + \frac{z^3}{\left(a^2 + z^2 \right)^{1.5}} \right] \tag{5}$$

where $\sigma_{1load} = \sigma_z$; $\sigma_{3load} = \sigma_r$; $Z = (t1 + t2 + t3)$, cm; uniform pressure, $q = P/A$, kN/m^2, where A = area, m^2; circular load, P = 40 kN; assume Poisson's ratio, $\nu = 0$ to 0.5

Thus, the total vertical and horizontal stress was calculated using Equations (6) and (7), respectively.

$$\sigma_1 = \sigma_{1pave} + \sigma_{1load} \tag{6}$$

$$\sigma_3 = \sigma_{3pave} + \sigma_{3load} \tag{7}$$

The principal stress (σ_1), confining stress (σ_3), cyclic stress/deviator (σ_d) stress, and bulk stress (θ or σ_b) were calculated as shown in Figure 5. Table 3 presents the in-situ stress for B278 and L72 from existing pavement conditions.

Figure 5. Schematic Diagram for Resilient Modulus Stress State.

Table 3. Summary of In Situ Stress.

Site ID	BH	Field Stress from Pavement (kPa)		Field Stress from Loading (kPa)		Total σ_1 (kPa)	Total σ_3 (kPa)	σ_d (kPa)	θ (kPa)
		σ_{1pave}	σ_{3pave}	σ_{1load}	σ_{3load}				
B278	B278-1	7.6	3.8	123.3	3.8	130.9	7.6	123.3	146.0
	B278-2	7.7	3.8	110.1	3.9	117.8	7.7	110.1	133.2
	B278-3	7.1	3.6	116.4	3.8	123.6	7.4	116.2	138.4
L72	L72-1	5.8	2.9	173.2	2.2	178.9	5.1	173.8	189.2
	L72-2	6.4	3.2	150.4	3.2	156.8	6.4	150.4	169.6
	L72-3	7.8	3.9	113.2	3.9	121.0	7.8	113.2	136.5
	L72-4	6.6	3.3	143.2	3.4	149.8	6.7	143.1	163.2
	L72-5	5.8	2.9	173.2	2.2	178.9	5.1	173.8	189.2
	L72-6	6.1	3.0	162.3	2.8	168.4	5.8	162.6	180.0
	L72-7	5.6	2.8	185.0	1.5	190.6	4.3	186.2	199.2
	L72-8	5.6	2.8	185.0	1.5	190.6	4.3	186.2	199.2
	L72-9	5.7	2.9	178.9	1.9	184.7	4.8	179.9	194.2
	L72-10	5.6	2.8	185.0	1.5	190.6	4.3	186.2	199.2
	L72-11	6.1	3.1	162.3	2.8	168.5	5.8	162.6	180.1

Note: BH = borehole.

3.4. Pavement Input Parameters

Table 4 summarizes the subgrade input parameters, which include the model parameters (k1, k2, and k3) for all boreholes at the two pavement sections and the corresponding resilient modulus, $M_{R(285)}$, found using the stress state per NCHRP-285 and the resilient modulus, $M_{R(in\,situ)}$, found using the in situ stress state.

Table 4. Summary of Materials Input.

Site ID	BH	k_1	k_2	k_3	$M_{R(285)}$ (MPa)	$M_{R\,(in\text{-}situ)}$ (MPa)	Initial IRI (mm/km)
B278	B278-1	520	0.923	1.281	55	132	1831 *
	B278-2	530	0.899	1.582	59	132	1752 *
	B278-3	555	0.934	0.131	48	80	1484
L72	L72-1	483	0.923	1.281	51	186	1121
	L72-2	413	1.154	0.769	38	114	963
	L72-3	430	0.913	1.082	44	90	821
	L72-4	470	0.933	1.230	49	139	616 *
	L72-5	871	0.440	−1.815	59	40	1073
	L72-6	690	0.228	1.010	80	141	1184
	L72-7	455	0.228	1.010	53	101	1247
	L72-8	445	0.219	1.052	52	101	1263
	L72-9	405	0.789	−0.714	31	44	1042
	L72-10	427	0.792	−1.100	31	37	1042
	L72-11	438	0.821	−1.210	31	36	1042

* PMED v2.6.2.2 limits the minimum initial IRI value to 789 mm/km and the maximum value to 1578 mm/km.

PG 64-22 grade AC input was selected as a Level 2 input, and the dynamic modulus value was obtained from laboratory testing per AASHTO T342 and categorized as Level 1 input. The remaining AC and base parameters were used as Level 3 for each pavement trial (PMED v2.6.2.2). The Modern Era Retrospective-Analysis for Research and Applications (MERRA) climate stations were selected for each pavement section. As part of the PMED process, the PMED (v2.6.2.2) program accesses the climate files associated with each station.

The files are each reported monthly, including temperature, wind speed, cloud cover, precipitation, and relative humidity. The traffic input parameters for PMED analysis were obtained from Islam and Gassman (2023) [28].

3.5. Threshold Values for Pavement Rutting and IRI

The threshold limit for the rutting and IRI are 12.7 mm and 3157 mm/km, respectively [3]. A ninety percent reliability level was considered for the PMED analysis. Historical records for the pavement sections included IRI measurements obtained periodically but did not include the initial IRI at the end of const ruction. Thus, linear regression was performed on the historical data to estimate the initial IRI for each pavement section. The initial IRI was found by extrapolating the data to the construction time. These values are summarized in Table 4 and categorized as Level 1.

4. Results

The effect of in situ stresses is discussed, and the resilient modulus testing results and the relation between $M_{R(285)}$ and $M_{R(in\ situ)}$ are presented. The predicted rutting and IRI values found using both M_{Rs} are discussed and compared to the field-measured values. Finally, the pavement section was classified based on rutting and IRI values per FHWA (2015).
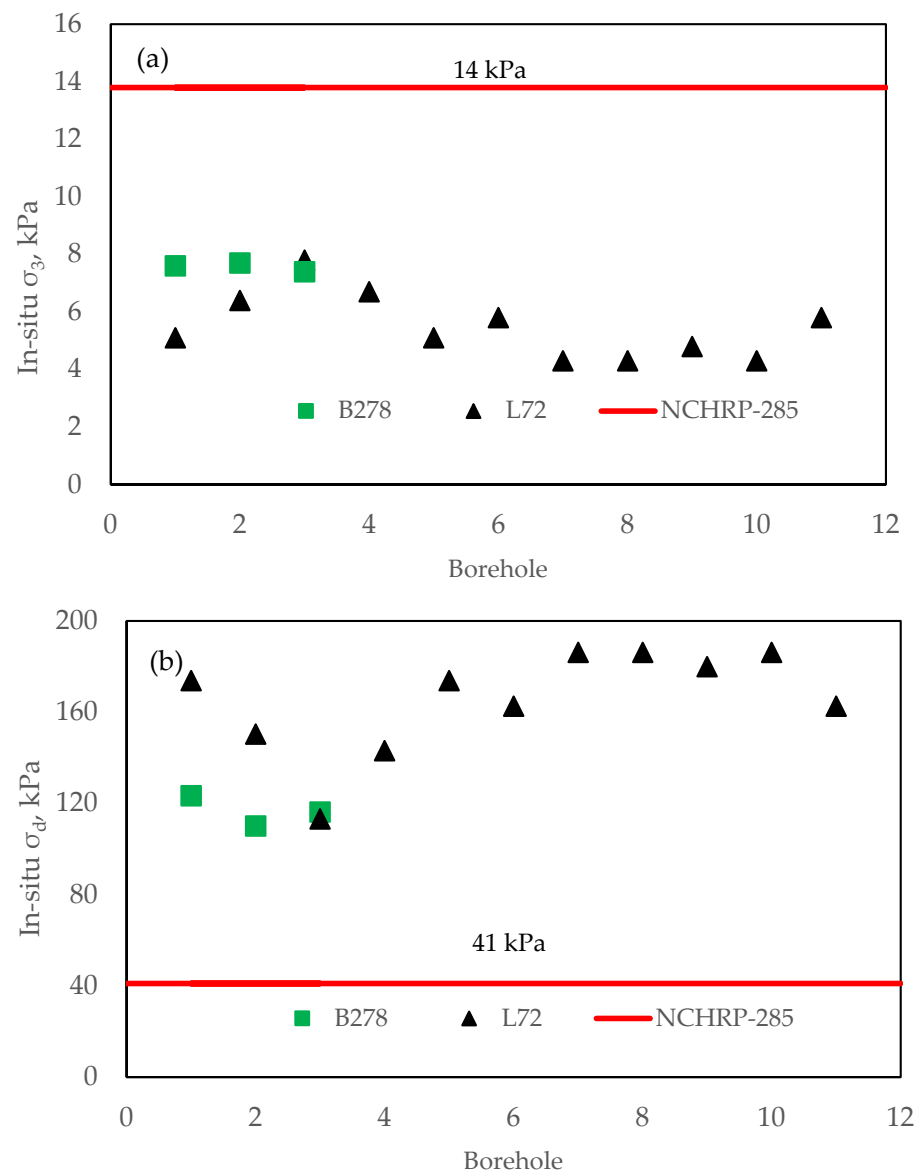
4.1. Effect of In Situ Stress

Figure 6 depicts the graphical comparison of in situ stress and stress recommended by NCHRP-285 [38]. As shown in Figure 6a, the in situ σ_3 is approximately 2.4 (average) times less than that of NCHRP-285. Similarly, as shown in Figure 6b, the in situ σ_d is approximately 3.8 (average) times higher than NCHRP-285 [38]. The σ_d is a function of vertical stress related to the pavement thickness. There is no vertical stress at zero thickness; vertical stress increases with increasing thickness.
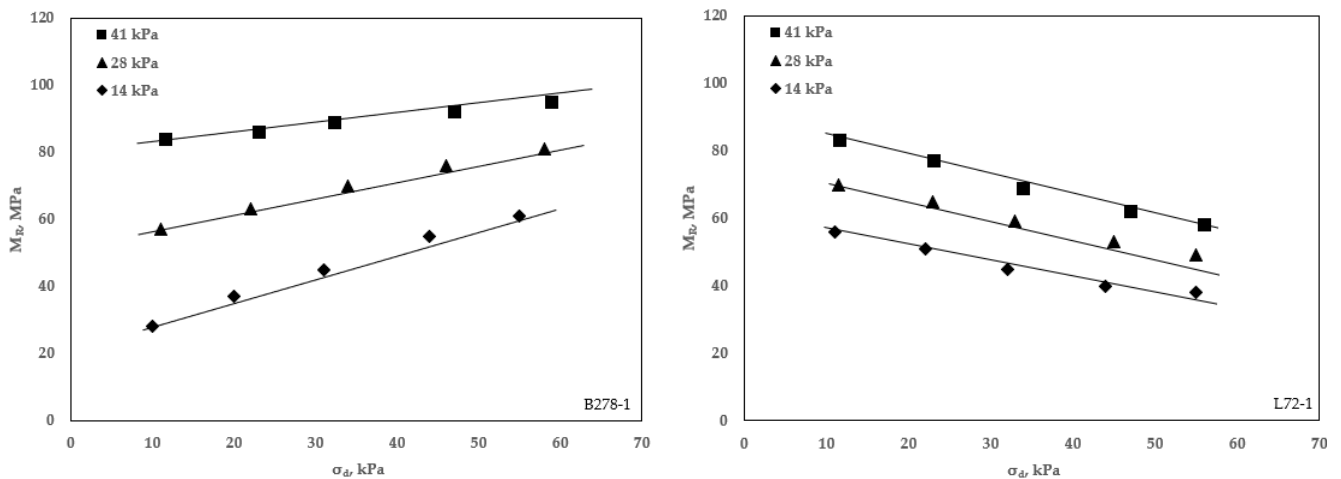
4.2. Resilient Modulus Test Result

To illustrate the results obtained from the repeated load triaxial tests that were performed on specimens at the in situ moisture content and density, Figure 7 presents M_R versus cyclic stress (deviator stress) at three different confining pressures (i.e., 41, 28, and 14 kPa) for tests performed for B278-1 (a coarse-grained soil) and L72-1 (a fine-grained soil). For B278-1, the results show that the M_R value increased with increasing cyclic (deviator) stress and exhibited higher M_R at higher confining pressure. This result was a good indication of granular materials as expected for A-1-b/SP soil. This is referred to as the 'strain-hardening' effect due to the reorientation of the grains into the denser state [30–34]. For the fine-grained soil at L72-1, the M_R decreased with increasing cyclic stress, and a lower M_R value was obtained. Other studies [15,16,33] have observed this decreasing trend in fine-grained soils. This is referred to as 'stress-softening' behavior; with increased stress, deformation increases, and the modulus decreases [30–34].

The average $M_{R(285)}$ and $M_{R(in\ situ)}$ for each pavement section are compared in Figure 8. These values were calculated as the average obtained for all boreholes along each section. Considering all of the AC pavement layer profiles studied herein, the average $M_{R(in\ situ)}$ is 1.1 to 2.1 (avg 1.4) times greater than the average $M_{R(285)}$, except for P93, which was 0.16 times less. That means in situ stress significantly influences the estimate of subgrade M_R.
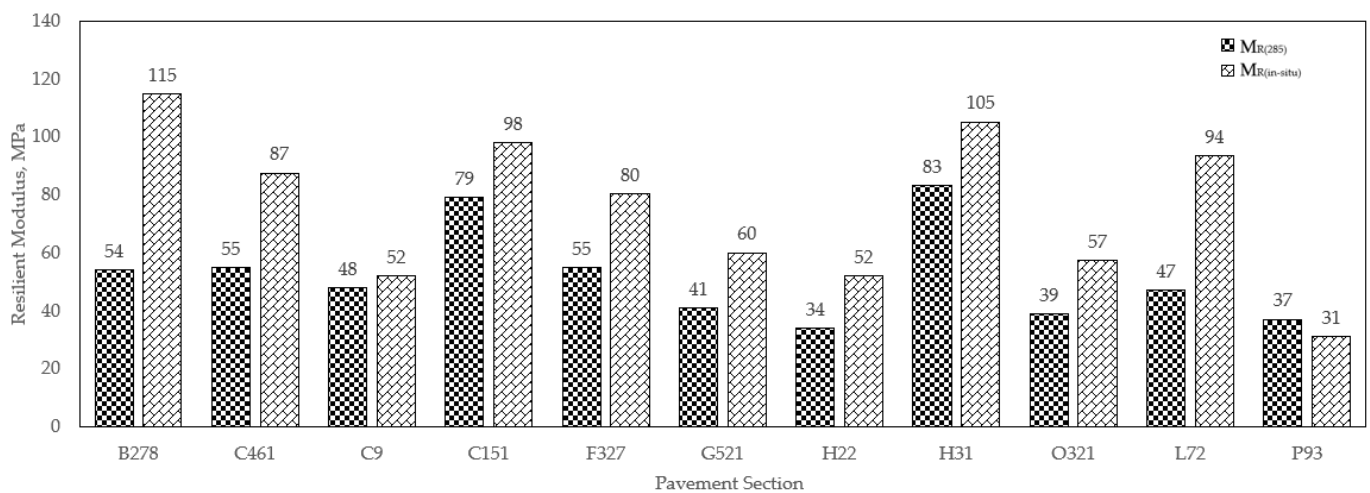
Figure 9 shows the correlation between $M_{R(in\ situ)}$ and $M_{R(285)}$ using all 73 samples. For this data, the bias = 24, the Pearson moment coefficient (r) = 0.65, and the standard error of estimate (SEE) = 2.68. The standard deviation and coefficient of variance are 20 and 38, respectively, for $M_{R(285)}$, but 37 and 48 for $M_{R(in\ situ)}$.
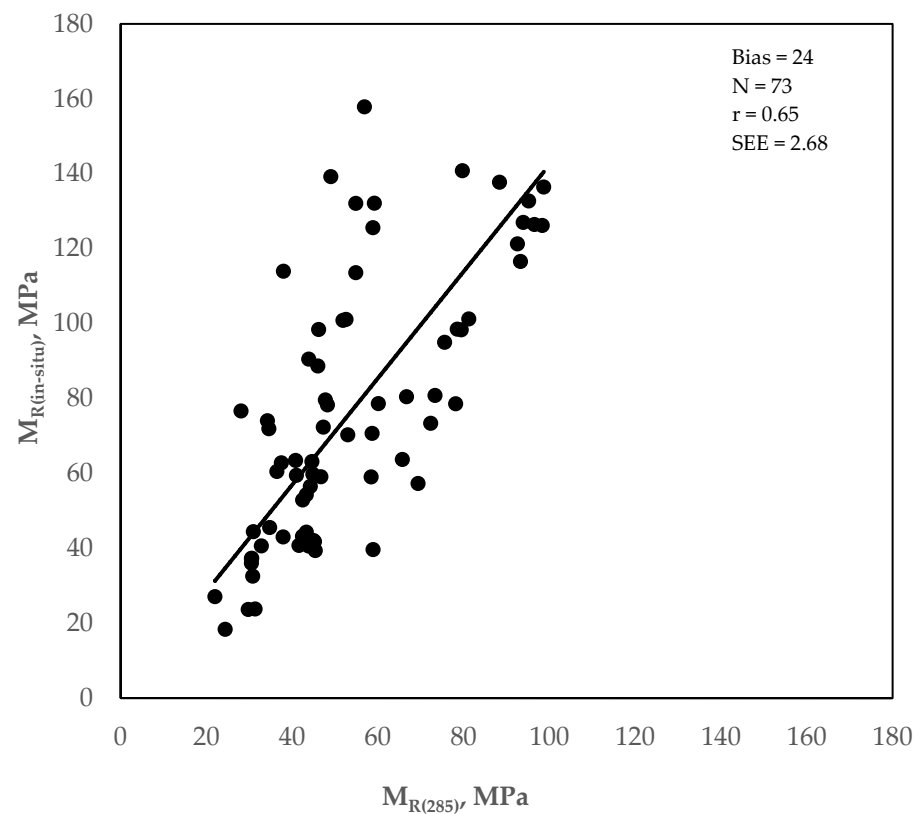
Figure 6. Effect of In Situ Stress for Sections B278 and L72: (**a**) In-situ Confining Pressure for each Borehole, and (**b**) In-situ Deviator Stress for each Borehole.

Figure 7. Effect of Confining Stress and Cyclic Stress on Subgrade M_R.

Figure 8. Comparison of the Average Resilient Modulus calculated using NCHRP-285 and the In Situ Stress.

Figure 9. Relation between $M_{R(285)}$ and $M_{R\,(in\,situ)}$ from all samples.

4.3. Effect of Subgrade M_R for Predicting Rutting and IRI

To address the objectives of this study, the predicted values of rutting and IRI were obtained from the AASHTOWare PMED software (v2.6.2.2) considering the two different subgrades M_R (e.g., $M_{R(285)}$ and $M_{R(in\,situ)}$).

Figure 10 illustrates the predicted and measured rutting as a function of pavement age for pavement segments B278-1 and L72-1. The FHWA rating system of "Good", "Fair", and "Poor" is also shown. The data indicate the following:

- For segment B278-1, the predicted rutting using $M_{R(in\,situ)}$ increased from 3 to 4.9 mm with pavement age. These values indicate that the pavement is in "Good" condition

for this period. The field-measured values have a similar magnitude and would also indicate that the pavement is in "Good" condition.

- The predicted rutting using $M_{R(285)}$ ranged from 5 to 7 mm, which is higher than predicted using $M_{R(in\ situ)}$ and indicates the pavement is in "Fair" condition. This is not in agreement with the "Good" rating from the field-measured values.
- Similar results were observed for segment L72-1, shown in Figure 9b. Furthermore, the predicted rutting for L72-1 using $M_{R(285)}$ indicates a "Fair" condition from 60 months to 216 months (18 years), whereas a "Fair" condition is not reached until 216 months (18 years) for the rutting predicted using $M_{R(in\ situ)}$.
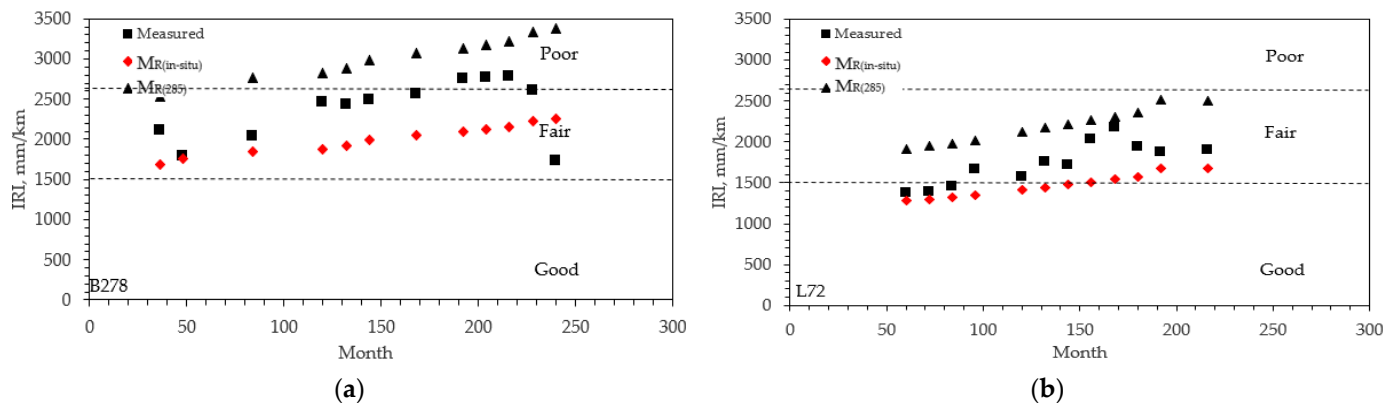

(a)   **(b)**

Figure 10. Effect of Subgrade M_R on Predicted Rutting (**a**) B278-1 and (**b**) L72-1. Note: 5.08 mm = "Good", 5.08–10.16 mm = "Fair", >10.16 mm = "Poor" FHWA (2015).

These observations indicate that both pavement segments were classified as "Fair" using the M_R found from NCHRP-285. In contrast, they were classified as "Good" using the M_R calculated using the in situ stress state. Furthermore, the classification from the predictions employing the M_R calculated using the in situ stress state agreed with the classification based on measure rutting. This illustrates the effect of stress conditions on calculating subgrade MR and, subsequently, using M_R in the rutting prediction.

Figure 11 illustrates the progression of predicted and measured IRI for segments B278-1 and L72-1 and provides the FHWA rating system based on the current condition for IRI. The data indicate the following:

- The initial IRI predicted for segment B278-1 is 1689 mm/km for $M_{R(in\ situ)}$ and 2533 mm/km for $M_{R(285)}$. Both values indicate that the pavement is in "Fair" condition.
- Using $M_{R(285)}$, the predicted IRI indicates that the B278-1 pavement is in "Poor" condition after 80 months, whereas using $M_{R(in\ situ)}$, the pavement is rated as "Fair" for the duration of the time studied.
- At 240 months, the predicted IRI of B278-1 was 2257 mm/km ("Fair" condition) for $M_{R(in\ situ)}$, but 3385 mm/km ("Poor" condition) for $M_{R(285)}$. That means the $M_{R(285)}$ predicted an IRI that was 1.5 times higher than predicted using the $M_{R(in\ situ)}$.
- The measured IRI values for B278-1 were between those predicted by $M_{R(285)}$ and $M_{R(in\ situ)}$. The measured values corresponded to an initial rating of "Fair" up to 192 months and "Poor" thereafter.
- For section L72-1, the predicted IRI using $M_{R(in\ situ)}$ was 1277 mm/km at 60 months and increased to 1671 mm/km at 216 months. Thus, this segment is initially rated as "Good" and then rated as "Fair" after 156 months. In contrast, when $M_{R(285)}$ is used, the predicted IRI is equal to 1915 mm/km at 60 months and increases to 2507 mm/km with a "Fair" rating for the duration studied.
- The measured IRIs for segment L72-1 were in between those predicted by $M_{R(285)}$ and $M_{R(in\ situ)}$ as they were for B278-1. At 216 months, the predicted IRI of L72-1 was 1671 mm/km ("Fair" condition) for $M_{R(in\ situ)}$, whereas 2507 mm/km ("Fair" condition)

for $M_{R(285)}$. That means the $M_{R(285)}$ predicted an IRI that was 1.5 times higher than predicted using the $M_{R(in\ situ)}$.

Figure 11. Effect of Subgrade M_R on Predicted IRI: (**a**) B278-1 and (**b**) L72-1. Note: 1500 mm/km = "Good", 1500–2680 mm/km = "Fair", >2680 mm/km = "Poor" FHWA (2015).

These observations indicate that the predicted IRI for B278-1 corresponded to a classification of "Poor" using the M_R found from NCHRP-285. In contrast, it was classified as "Fair" using the M_R calculated using the in situ stress state. Similarly, for $M_{R(in\ situ)}$, the section of L72-1 was initially classified as "Good", and it is rated as "Fair" after 150 months; the section was classified as a "Fair" rating for the duration studied for $M_{R(285)}$. Furthermore, the $M_{R(in\ situ)}$ predicted 33% less IRI for both sections than the $M_{R(285)}$. When $M_{R(in\ situ)}$ was used, the predicted IRI was, on average, 17% (less) than in the field-measured values, whereas $M_{R(285)}$ overpredicted the IRI by 21%.

5. Summary of Findings and Conclusions

This study investigated the prediction of rutting and IRI for flexible pavement considering the two different subgrade resilient moduli (i.e., $M_{R(285)}$ & $M_{R(in\ situ)}$). The results are summarized below:

1. Based on the resilient modulus test results, the M_R of coarse-grained soil increases with increasing deviator stress. In contrast, the M_R of fine-grained soil decreases with increasing deviator stress because of the "stress hardening" and "stress softening" behavior for coarse-grained and fine-grained soil, respectively.
2. Rutting: Both sections were classified as "Fair" using the M_R found from NCHRP-285, whereas they were classified as "Good" employing the M_R calculated using the in situ stress state. The reason is that the in situ stress significantly affects the calculation of subgrade M_R and, subsequently, the use of M_R in the rutting prediction. The predictions using $M_R(in\ situ)$ were in close agreement with the field-measured values.
3. IRI: For both sections, the predicted IRI using $M_{R(in\ situ)}$ was 33% less than the IRI predicted using $M_{R(285)}$. Section B278-1 was classified as "Fair" using the M_R found from the in situ stress state, whereas it was rated as "Poor" using the M_R calculated using the NCHRP-285. Similarly, the section of L72-1 was classified as "Fair" for the duration studied for $M_{R(285)}$. In contrast, it was initially classified as "Good", and it is rated as "Fair" after 150 months of using $M_{R(in\ situ)}$. The predicted IRI was approximately 17% (average) less than in the field-measured values when the $M_R(in\ situ)$ was used, whereas 21% was overpredicted using $M_{R(285)}$.

Therefore, in situ stress should be considered to predict rutting and IRI for flexible pavement.

Author Contributions: Conceptualization, Methodology, Software, Validation, Writing—Original draft, Writing—review, and editing, K.M.I.; Conceptualization, Methodology, Writing—review and editing, S.L.G. All authors have read and agreed to the published version of the manuscript.

References

1. AASHTO. *Guide for Design of Pavement Structures*; AASHTO: Washington, DC, USA, 1993.
2. AASHTO. *Mechanistic-Empirical Pavement Design Guide: A Manual of Practice*, 2nd ed.; AASHTO: Washington, DC, USA, 2015.
3. AASHTO. *Mechanistic-Empirical Pavement Design Guide: A Manual of Practice*, 3rd ed.; AASHTO: Washington, DC, USA, 2020.
4. Seed, H.B.; Chan, C.K.; Lee, C.E. Resilience Characteristics of Subgrade Soils and their Relations to Fatigue Failures in Asphalt Pavements. In Proceedings of the International Conference on the Structural Design of Asphalt Pavements, Ann Arbor, MI, USA, 20–24 August 1962; pp. 77–113.
5. Brown, S.F. Soil Mechanics in Pavement Engineering, 36th Rankine Lecture of the British Geotechnical Society. *Geotechnique* **1996**, *46*, 383–426. [CrossRef]
6. Ng, K.; Henrichs, Z.R.; Ksaibati, K.; Wulff, S.S. Measurement and Estimation of the Resilient Modulus of Subgrade Materials for Mechanistic-Empirical Pavement Design Guide in Wyoming. In Proceedings of the Transportation Research Board Annual Meeting, Washington, DC, USA, 10–14 January 2016; pp. 1–17.
7. Brown, S.F. Repeated Load Testing of a Granular Material. *J. Geotech. Eng. Div.* **1974**, *100*, 825–841. [CrossRef]
8. Burczyk, J.M.; Ksaibati KSprecher, R.A.; Farrar, M.J. Factors Influencing Determination of a Subgrade Resilient Modulus Value. In *Transportation Research Record 1462*; Transportation Research Board, National Research Council: Washington, DC, USA, 1995; pp. 72–78.
9. Burmister, D.M. *The Theory of Stresses and Displacements in Layered Systems and Application to the Design of Airport Runways. Highway Research Board*; National Research Council: Washington, DC, USA, 1943; Volume 23, pp. 125–148.
10. Ng, K.; Hellrung, D.; Ksaibati, K.; Wulff, S.S. Systematic back-calculation protocol and prediction of resilient modulus for MEPDG. *IJPE* **2018**, *19*, 62–74. [CrossRef]
11. *AASHTO T 307*; Standard Method of Test for Determining the Resilient Modulus of Soils and Aggregate Materials. AASHTO: Washington, DC, USA, 2017.
12. Puppala, A.; Mohammad, L.; Allen, A. Engineering Behavior of Lime-Treated Louisiana Subgrade Soil. *Transp. Res. Rec. J. Transp. Res. Board* **1996**, *1546*, 24–31. [CrossRef]
13. Puppala, A.J. *Estimating Stiffness of Subgrade and Unbound Materials for Pavement Design*; Transportation Research Board: Washington, DC, USA, 2008.
14. Han, Z.; Vanapalli, S.K. State-of-the-Art: Prediction of Resilient Modulus of Unsaturated Subgrade Soils. *Int. J. Geomech.* **2016**, *16*, 04015104. [CrossRef]
15. Islam, K.M.; Gassman, S.; Rahman, M.M. Field and laboratory characterization of subgrade resilient modulus for pavement mechanistic-empirical pavement design guide application. *TRB* **2020**, *2674*, 921–930. [CrossRef]
16. Rahman, M.M.; Islam, K.M.; Gassman, S. Estimation of resilient modulus for coarse-grained subgrade soils from quick shear tests for mechanistic-empirical pavement designs. *Designs* **2019**, *3*, 48. [CrossRef]
17. Islam, K.M.; Gassman, S.L. Influence of subgrade resilient modulus selection methodology on AASHTOWare pavement ME design. In *Geo-Congress*; ASCE: Charlotte, North Carolina, 2022; pp. 192–204.
18. Rahman, M.M.; Gassman, S.L.; Islam, K.M. Effect of Moisture Content on Subgrade Soils Resilient Modulus for Predicting Pavement Rutting. *Geosciences* **2023**, *13*, 103. [CrossRef]
19. Seed, H.; Mitry FMonosmith, C.; Chan, C. Prediction of Pavement Deflection From Laboratory Repeated Load Tests. In *Report No. 35*; NCHRP, Transportation Research Board: Washington, DC, USA, 1967.
20. Yao, Y.; Zheng, J.; Zhang, J.; Peng, J.; Li, J. Model for predicting resilient modulus of unsaturated subgrade soils in south China. *KSCE J. Civ. Eng.* **2018**, *22*, 2089–2098. [CrossRef]
21. Zhang, J.; Peng, J.; Zeng, L.; Li, J.; Li, F. Rapid estimation of resilient modulus of subgrade soils using performance-related soil properties. *Int. J. Pavement Eng.* **2021**, *22*, 732–739. [CrossRef]
22. Tamošiūnas, T.; Skuodis, Š. Predictive Stress Modeling of Resilient Modulus in Sandy Subgrade Soils. *Infrastructures* **2023**, *8*, 29. [CrossRef]
23. Kumar, P.; Puppala, A.J.; Tingle, J.S.; Chakraborty, S.; Congress, S.S.C. Resilient Characteristics of Polymer Emulsion-Treated Sandy Soil. *Transp. Res. Rec.* **2022**, *2676*, 526–538. [CrossRef]

24. Zhang, J.; Peng, J.; Liu, W.; Lu, W. Predicting resilient modulus of fine-grained subgrade soils considering relative compaction and matric suction. *Road Mater. Pavement Des.* **2021**, *22*, 703–715. [CrossRef]
25. Kim, S.S.; Pahno, S.; Durham, S.A.; Yang, J.; Chorzepa, M.G. *Prediction of Resilient Modulus From the Laboratory Testing of Sandy Soils (No. FHWA-GA-19-1725)*; Department of Transportation. Office of Performance-Based Management & Research: Atlanta, GA, USA, 2019; Georgia DOT Research project 17–25, Final Report.
26. Mohammad, L.N.; Huang BPuppala, A.J.; Allen, A. Regression Model for Resilient Modulus of Subgrade Soils. *Transp. Res. Rec. J. Transp. Res. Board* **1999**, *1687*, 47–54. [CrossRef]
27. Bhuvaneshwari, S.; Robinson, R.G.; Gandhi, S.R. Resilient Modulus of Lime Treated Expansive Soil. *Geotech. Geol. Eng.* **2018**, *37*, 305–315. [CrossRef]
28. Islam, K.M.; Gassman, S.L. Predicting Flexible Pavement Distress and IRI Considering Subgrade Resilient Modulus of Fine-Grained Soils Using MEPDG. *Materials* **2023**, *16*, 1126. [CrossRef] [PubMed]
29. Rada, G.; Witczak, M.W. Comprehensive Evaluation of Laboratory Resilient Moduli Results for Granular Materials. In *Transportation Research Record 810*; TRB, National Research Council: Washington, DC, USA, 1981; pp. 23–33.
30. Buchanan, S. Resilient modulus: What, Why, and How? 2007. Available online: https://www.vulcaninnovations.com/public/pdf/2-Resilient-Modulus-Buchanan.pdf (accessed on 1 February 2023).
31. Drumm, E.C.; Boateng-Poku, Y.; Johnson Pierce, T. Estimation of subgrade resilient modulus from standard tests. *J. Geotech. Eng.* **1990**, *116*, 774–789. [CrossRef]
32. Kumar, A.; George, V. Effect of soil parameters on resilient modulus using cyclic tri-axial tests on lateritic subgrade soils from Dakshina Kannada, India. *Geotech. Geol. Eng.* **2018**, *36*, 3987–4000. [CrossRef]
33. Maher, A.; Bennert, T.; Gucunski, N.; Papp, W.J., Jr. *Resilient Modulus Properties of New Jersey Subgrade Soils (No. FHWA NJ 2000-01)*; FHWA NJ 2000-01, Final Report; TRIS, USDOT, STATEDOT: Washington, DC, USA, 2000.
34. Kim, D.; Siddiki, N.Z. Simplification of resilient modulus testing for subgrades. *Jt. TRP* **2006**, *265*, IN/JTRP-2005/23. Available online: https://docs.lib.purdue.edu/cgi/viewcontent.cgi?article=1736&context=jtrp (accessed on 1 February 2023).
35. Witzack, M.; Qi, X.; Mirza, M.W. Use of Nonlinear Subgrade Modulus in AASHTO Design Procedures. *J. Transp. Eng.* **1995**, *121*, 273–282.
36. Yau, A.; Von Quintus, H. *Study of LTPP Laboratory Resilient Modulus Test Data and Response Characteristics*; Report No. FHWA-RD-02-051; Federal Highway Administration: McLean, VA, USA, 2002.
37. Zaman, M.; Chen, D.-H.; Laguros, J. Resilient Modulus of Granular Materials. *J. Transp. Eng.* **1994**, *120*, 967–988. [CrossRef]
38. NCHRP-285. *Laboratory Determination of Resilient Modulus for Flexible Pavement Design*; Research Results Digest, Issue Number 14; Transportation Research Board: Washington, DC, USA, 2004; 486p.
39. Fesearal Highway Administration (FHWA). Pavement Performance Measures and Forecasting and The Effects of Maintenance and Rehabilitation Strategy on Treatment Effectiveness, Chapter 3, 2015. Available online: https://www.fhwa.dot.gov/publications/research/infrastructure/pavements/ltpp/17095/004.cfm (accessed on 1 February 2023).
40. Amirkhanian, S.N.; Corley, M. *Characterization of Bases and Subbases for AASHTO ME Pavement Design (No. FHWA-SC-21-01)*; Tech Report; South Carolina. Dept. of Transportation. Office of Materials and Research, Tri-County Technical College: Pendleton, UC, USA, 2021.
41. Hurley, C.D. Asphalt Pavement Evaluation to Support the Calibration of the AASHTO MEPDG for South Carolina Conditions. Master Thesis, Clemson University, Clemson, SC, USA, 2019; ProQuest LLC, Ann Arbor, MI 48106-1346.
42. *NCHRP-1-37*; Guide for Mechanistic-Empirical Design of New and Rehabilitated Pavement Structures-Final Report. Transportation Research Board: Washington, DC, USA, 2004.
43. Huang, Y.H. *Pavement Analysis and Design*; Prentice Hall, Inc.: Englewood Cliffs, NJ, USA, 1993.